Molecular Cell
Article

Coupling of Ribosomal L1 Stalk and tRNA Dynamics during Translation Elongation

Jingyi Fei,[1] Pallav Kosuri,[2] Daniel D. MacDougall,[1] and Ruben L. Gonzalez, Jr.[1,*]
[1]Department of Chemistry
[2]Department of Biochemistry and Molecular Biophysics
Columbia University, New York, NY 10027, USA
*Correspondence: rlg2118@columbia.edu
DOI 10.1016/j.molcel.2008.03.012

SUMMARY

By using single-molecule fluorescence resonance energy transfer (smFRET), we observe the real-time dynamic coupling between the ribosome, labeled at the L1 stalk, and transfer RNA (tRNA). We find that an interaction between the ribosomal L1 stalk and the newly deacylated tRNA is established spontaneously upon peptide bond formation; this event involves coupled movements of the L1 stalk and tRNAs as well as ratcheting of the ribosome. In the absence of elongation factor G, the entire pretranslocation ribosome fluctuates between just two states: a nonratcheted state, with tRNAs in their classical configuration and no L1 stalk-tRNA interaction, and a ratcheted state, with tRNAs in an intermediate hybrid configuration and a direct L1 stalk-tRNA interaction. We demonstrate that binding of EF-G shifts the equilibrium toward the ratcheted state. Real-time smFRET experiments reveal that the L1 stalk-tRNA interaction persists throughout the translocation reaction, suggesting that the L1 stalk acts to direct tRNA movements during translocation.

INTRODUCTION

One of the most dynamic aspects of protein synthesis is the movement of transfer RNA (tRNA) and messenger RNA (mRNA) substrates through the ribosome during the elongation cycle of translation. X-ray crystallographic structures have defined three "classical" tRNA-binding sites that span the intersubunit space of the ribosome, with the tRNAs arranged such that their anticodon ends are held in distinct aminoacyl- (A), peptidyl- (P), and deacylated-tRNA, or exit (E), binding sites within the small ribosomal subunit (30S in *Escherichia coli*), while their acceptor ends are held at corresponding A, P, and E sites within the large ribosomal subunit (50S in *E. coli*) (Korostelev et al., 2006; Selmer et al., 2006). During elongation, aminoacyl-tRNAs are initially delivered to the A site and subsequently transit into the P and E sites before dissociating from the translating ribosome.

In addition to the classical tRNA configurations, early chemical modification experiments identified an intermediate "hybrid" configuration of the tRNAs (Moazed and Noller, 1989). The hybrid configuration is populated spontaneously upon peptide bond formation and is characterized by displacement of the acceptor ends of the newly deacylated P site tRNA and the newly formed peptidyl A site tRNA into the E and P sites on the 50S subunit, respectively, while their anticodon ends remain fixed in the P and A sites on the 30S subunit (Moazed and Noller, 1989). Translocation of the tRNA anticodon-mRNA codon complex on the 30S subunit, leading to completion of one elongation cycle, is then catalyzed by the GTPase and ribosomal translocase, elongation factor G (EF-G) (Spirin, 1985).

Cryo-electron microscopy (cryo-EM) reconstructions of ribosomal complexes imaged in the absence and presence of a biochemically trapped EF-G have revealed large-scale conformational changes of the ribosome that the authors suggest are induced by EF-G binding (Connell et al., 2007; Frank and Agrawal, 2000; Valle et al., 2003). Two of the major conformational changes observed are a counterclockwise rotation of the 30S subunit relative to the 50S subunit, termed ratcheting, and an ~20 Å movement of the ribosomal L1 stalk into the intersubunit space, toward the tRNA binding sites (Connell et al., 2007; Frank and Agrawal, 2000; Valle et al., 2003). Temporal and functional correlation of these observed conformational changes of the ribosome with each other and with the movement of tRNAs and mRNA through the ribosome remains a major goal of mechanistic studies of the translation elongation cycle.

The ribosomal L1 stalk is a universally conserved and highly dynamic structural feature of the 50S subunit that is composed of ribosomal protein L1 and helices 76–78 of the large subunit 23S ribosomal RNA (Figure 1A). A very suggestive feature of the conformational changes visualized in the cryo-EM studies is the observation, in the EF-G-bound ribosomal complex, of a direct interaction between the L1 stalk and the central fold domain, or elbow, of the deacylated tRNA residing in the hybrid P/E (denoting 30S P/50S E) configuration. Observation of this interaction has led to the untested hypothesis that the L1 stalk might be directly involved in translocation of the newly deacylated tRNA from the P to the E site (Valle et al., 2003). Taken together, the currently available chemical modification data have established that formation of the hybrid P/E tRNA configuration occurs independently of EF-G binding (Moazed and Noller, 1989), while the cryo-EM data suggest that movement of the L1 stalk and formation of the L1 stalk-P/E tRNA intermolecular contact are induced upon binding of EF-G (Valle et al., 2003). Experimental correlation of the classical-to-hybrid tRNA transition, the binding

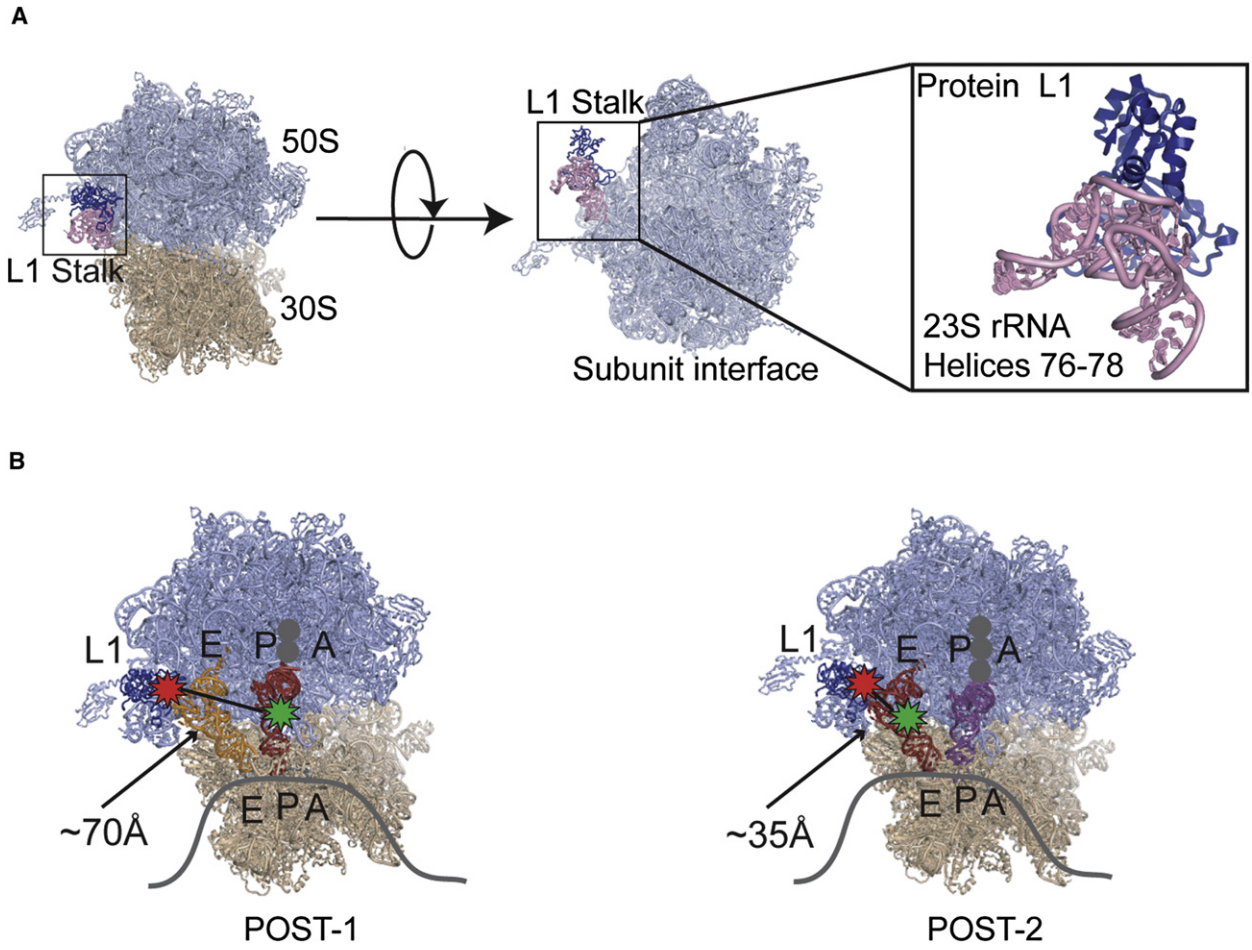

Figure 1. Structure and Fluorescence Labeling of the Ribosomal L1 Stalk

(A) X-ray crystallographic structure of the 70S ribosome (Protein Data Bank [PDB] ID, 2J00 and 2J01) and the L1 stalk (PDB ID, 1MZP). The 50S subunit is shown in lavender and the 30S subunit in tan. Helices 76–78 of 23S rRNA are shown in pink, and the L1 protein is in dark blue.

(B) Approximate positions of the donor and acceptor fluorophores in the ribosome complexes we have investigated. The donor (Cy3) and acceptor (Cy5) fluorophores are marked as green and red stars, respectively. The Cy3-labeled tRNA is shown in red. The distances between L1(Cy5) and P site-bound (Cy3)tRNA (~70 Å, left panel) and E site-bound (Cy3)tRNA (~35 Å, right panel), as measured from the X-ray crystallographic structure of the 70S ribosome, are marked by a black line.

of EF-G, and the formation of the intermolecular L1 stalk-tRNA contact should allow testing of this hypothesis as well as the development of a mechanistic model for the role of the L1 stalk in translocation.

Recently, single-molecule fluorescence resonance energy transfer (smFRET) experiments utilizing fluorescently labeled A and P site tRNAs have provided a very effective means of monitoring the conformational dynamics of tRNAs during the classical-to-hybrid transition (Blanchard et al., 2004; Kim et al., 2007; Munro et al., 2007). These experiments have unequivocally established that, on the pretranslocation ribosome and in the absence of EF-G, tRNAs exist in a dynamic equilibrium between the classical and hybrid configurations (Blanchard et al., 2004; Kim et al., 2007; Munro et al., 2007). However, because it does not utilize a fluorescent probe on the ribosome itself, the tRNA-tRNA smFRET signal is unable to directly report on conformational dynamics of the ribosome.

In order to directly correlate ribosome and tRNA conformational dynamics experimentally, we report the use of smFRET to directly monitor the interaction of the ribosome, labeled at the L1 stalk, with tRNA during a full elongation cycle. Contrary to interpretations of cryo-EM structures (Valle et al., 2003), we find that the interaction between the L1 stalk and the hybrid P/E tRNA is established spontaneously and rapidly upon peptide bond formation, with no requirement for EF-G binding. In the absence of EF-G, the pretranslocation ribosomal complex is highly dynamic, fluctuating between two distinct conformations in which the intermolecular contact between the L1 stalk and hybrid P/E tRNA is alternately formed and disrupted. Taken together with cryo-EM (Valle et al., 2003) and bulk FRET studies (Ermolenko et al., 2007), our smFRET signal strongly suggests that the entire pretranslocation ribosome fluctuates between just two global conformational states: a nonratcheted state, with tRNAs in their classical configuration and no interaction

between the L1 stalk and the deacylated P/P tRNA, and a ratcheted state, with tRNAs in their hybrid configuration and a direct interaction between the L1 stalk and the deacylated P/E tRNA.

The L1 stalk-tRNA smFRET signal allows us to assess how the presence, and acylation state, of an A site tRNA substrate affects the energetics of the equilibrium between the two global conformational states of the pretranslocation complex. Binding of EF-G to the fluctuating pretranslocation complex provides directionality, shifting the equilibrium such that the ratcheted state is favored, effectively trapping the ribosomal complex in this state and blocking the reverse transition. Real-time smFRET experiments reveal that the L1 stalk remains associated to the tRNA throughout translocation and thus escorts the tRNA from the hybrid P/E to the classical E/E configuration. Our data strongly suggest that formation and maintenance of the L1 stalk-P/E tRNA contact are critical mechanistic features of translocation.

RESULTS AND DISCUSSION

Introduction of a Single, Site-Specific Fluorophore into the Ribosomal L1 Stalk and Preparation of Posttranslocation Complexes

In order to correlate ribosome and tRNA dynamics during translation elongation, an smFRET acceptor fluorophore (Cy5) was site-specifically introduced into ribosomal protein L1, and L1(Cy5) was reconstituted into ribosomes lacking wild-type L1 (referred to as L1[−], see Figures S1 and S2 available online) (Odom et al., 1990). We estimate ~60% labeling efficiency of L1, ~100% reconstitution of L1 into L1(−) ribosomes, and thus an overall ~60% labeling efficiency of ribosomes. L1(Cy5)-labeled ribosomes retain wild-type translation elongation activity in a standard primer-extension inhibition, or "toeprinting," assay (Hartz et al., 1988) (Figure S3). Ribosomes harboring an unlabeled L1 or lacking L1 are not observable in our experimental setup and therefore do not affect the collected smFRET data or its analysis. For detailed information regarding the preparation and functional testing of fluorescently labeled ribosomes, please see the Supplemental Experimental Procedures.

The donor fluorophore (Cy3) was conjugated to the elbow region of $tRNA^{Phe}$ at the naturally occurring 3-(3-amino-3-carboxy-propyl) uridine residue at position 47, and the resulting (Cy3)$tRNA^{Phe}$ was purified to homogeneity as previously described (Blanchard et al., 2004). Using these fluorescent reagents in our highly purified in vitro translation system (Blanchard et al., 2004), we then enzymatically prepared a posttranslocation elongation complex (POST-1) containing OH-$tRNA^{fMet}$ in the E site, fMet-Phe-(Cy3)$tRNA^{Phe}$ in the P site, and an empty A site (Figure 1B). For further details regarding preparation of POST-1, please see the Experimental Procedures.

Posttranslocation Complexes Are Compositionally Heterogeneous

We have used biochemical and single-molecule methods to assess two potential sources of compositional heterogeneity in our posttranslocation ribosomal complexes. The first of these is incomplete reactivity, in which complexes fail to either form a peptide bond or undergo translocation. Toeprinting reactions indicate that initiated L1(Cy5) ribosomes are ~95% competent for participation in the first round of elongation and 80%–85% competent for participation in the second round (Figure S3); analysis of subpopulations detected in our smFRET experiments is consistent with this observation (Figure 2C).

The second source of compositional heterogeneity arises from the instability of E site tRNA binding to posttranslocation ribosomes (Semenkov et al., 1996). To directly measure the stability of E site tRNA binding following translocation, we stopped-flow delivered a solution of ternary complex composed of elongation factor Tu (EF-Tu), GTP, and Lys-$tRNA^{Lys}$ with EF-G(GTP) to surface-immobilized POST-1. Upon Lys-$tRNA^{Lys}$ incorporation into POST-1 and translocation, OH-(Cy3)$tRNA^{Phe}$ moves into the E site; its lifetime prior to dissociation can then be obtained by monitoring the time-resolved disappearance of OH-(Cy3)$tRNA^{Phe}$ from POST-1 (Experimental Procedures, Figure S4). Exponential fits to time-resolved population histograms of the Cy3 signal reveal the existence of two populations of complexes. Approximately 34% of the complexes display a relatively rapid loss of the Cy3 signal, with a lifetime (τ) of 22 ± 1 s, indicating a relatively unstably bound OH-(Cy3)$tRNA^{Phe}$. The remaining ~66% of the complexes display a slower loss of Cy3 signal, with the actual lifetime measurement limited by the rate of Cy3 photobleaching under our experimental conditions ($\tau \geq 330 \pm 10$ s). Complexes in this slower population have either failed to undergo peptide bond formation or translocation (~20%, Figure S3) or have a stably bound OH-(Cy3)$tRNA^{Phe}$ (~66% − ~20% ≈ 46%) at the E site. We verified that the loss of Cy3 signal was indeed due to E site tRNA dissociation by demonstrating a previously reported buffer dependence of E site tRNA stability (Semenkov et al., 1996) (data not shown).

In summary, under our experimental conditions, posttranslocation complexes are compositionally heterogeneous and contain three subpopulations: ~20% are unreacted complexes, ~34% of the complexes are posttranslocated with an empty E site, and ~46% are posttranslocated with a deacylated tRNA at the E site. We have accounted for this compositional heterogeneity when interpreting our single-molecule experiments.

The L1 Stalk Is Conformationally Heterogeneous Relative to the Classical P/P tRNA in a Posttranslocation Complex

We first monitored the smFRET signal in POST-1 between L1(Cy5) and fMet-Phe-(Cy3)$tRNA^{Phe}$ in the classical P/P configuration (Figure 1B). We observed a low smFRET signal centered at 0.2 FRET with a broad distribution spanning between 0 and 0.4 FRET (Figure 2A). There are two potential origins of this wide distribution of smFRET values. The first is compositional heterogeneity with respect to tRNA occupancy of the E site as described above. The second is conformational heterogeneity of the L1 stalk; such conformational heterogeneity has been observed in ribosomes with a vacant E site (Frank and Agrawal, 2000; Schuwirth et al., 2005), and comparison of cryo-EM (Valle et al., 2003) and crystal (Korostelev et al., 2006; Selmer et al., 2006; Yusupov et al., 2001) structures of ribosomal complexes suggests conformational heterogeneity of the L1 stalk even in the presence of an E site tRNA. Given the long distance between the L1 stalk and the classical P/P tRNA, the observed low FRET efficiency is outside of the range in which FRET is most sensitive

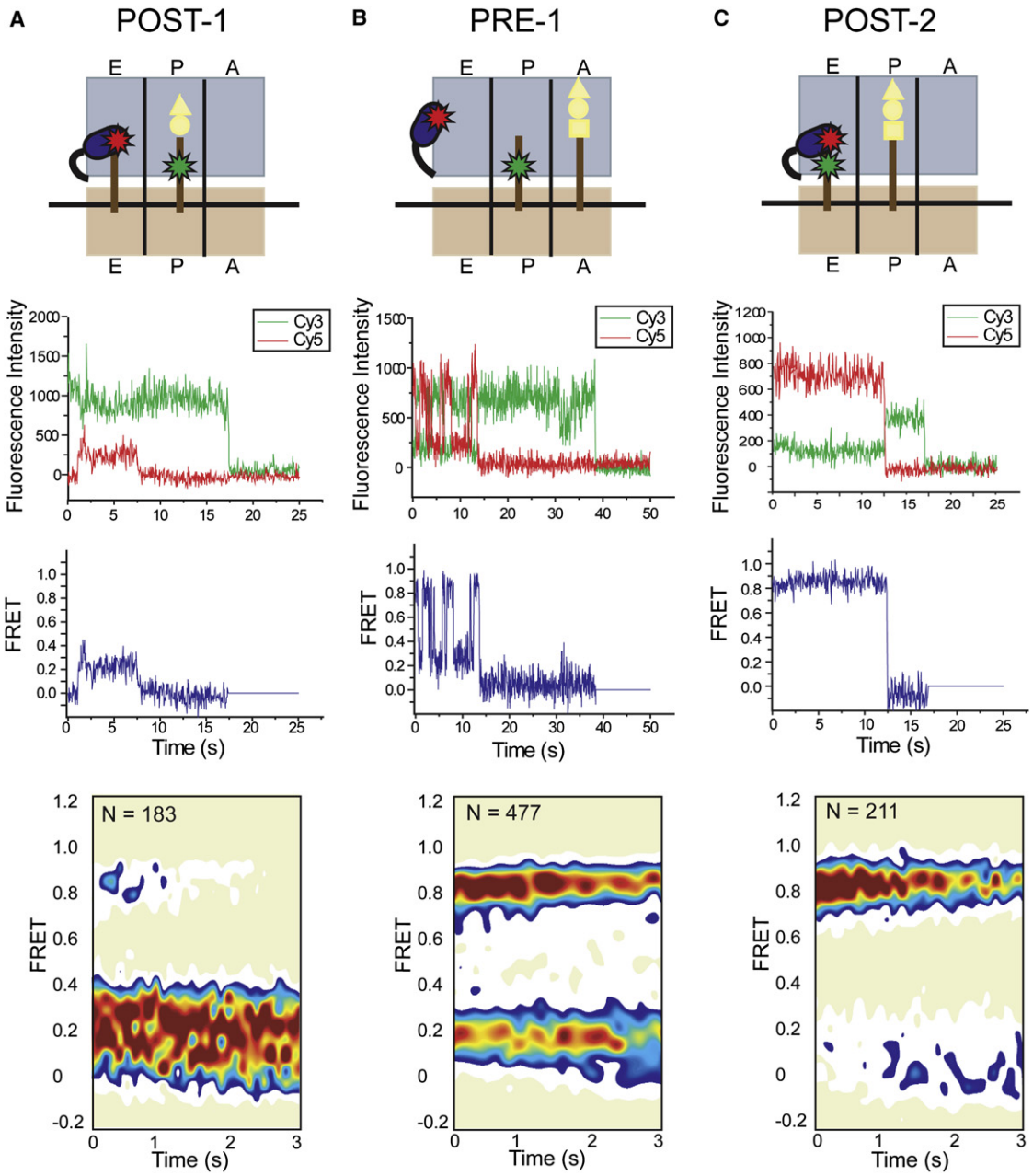

Figure 2. Steady-State smFRET Measurements of POST-1, PRE-1, and POST-2

Cartoon representations of the various complexes depict the 30S and 50S subunits in tan and lavender, respectively, with the L1 stalk in dark blue, the tRNAs as brown lines, and the Cy3 and Cy5 fluorophores as green and red stars, respectively (first row). Representative Cy3 and Cy5 emission intensities are shown in green and red, respectively (second row). The corresponding smFRET traces, $I_{Cy5}/(I_{Cy3} + I_{Cy5})$, are shown in blue (third row). Contour plots of the time evolution of population FRET are generated by superimposing the individual smFRET time traces (fourth row). Contours are plotted from tan (lowest population) to red (highest population). The number of traces that were used to construct each contour plot is indicated by "N." (A) POST-1. The small amount of density centered at 0.84 in this complex arises from a few traces in which spontaneous hydrolysis of the dipeptide at the P site results in fluctuations to the 0.84 FRET state. (B) PRE-1, generated by addition of 100 nM EF-Tu(GTP)Lys-tRNA^{Lys} to POST-1. Only traces that sample both the 0.21 and 0.84 FRET states, consistent with binding of EF-Tu(GTP)Lys-tRNA^{Lys} and peptide-bond formation, were included in the contour plot (~70% of the observed traces). (C) POST-2, generated by addition of 100 nM EF-Tu(GTP)Lys-tRNA^{Lys} and 1 μM EF-G(GTP) to POST-1. Only traces that stably sample the 0.84 FRET state, consistent with undergoing the full elongation reaction and retaining an E site bound OH-tRNA^{Phe} (~67% of the observed traces), are included in the contour plot. Lifetime analysis of the remaining 33% of the traces confirms that they arise from complexes that either did not bind EF-Tu(GTP)Lys-tRNA^{Lys} or did not translocate.

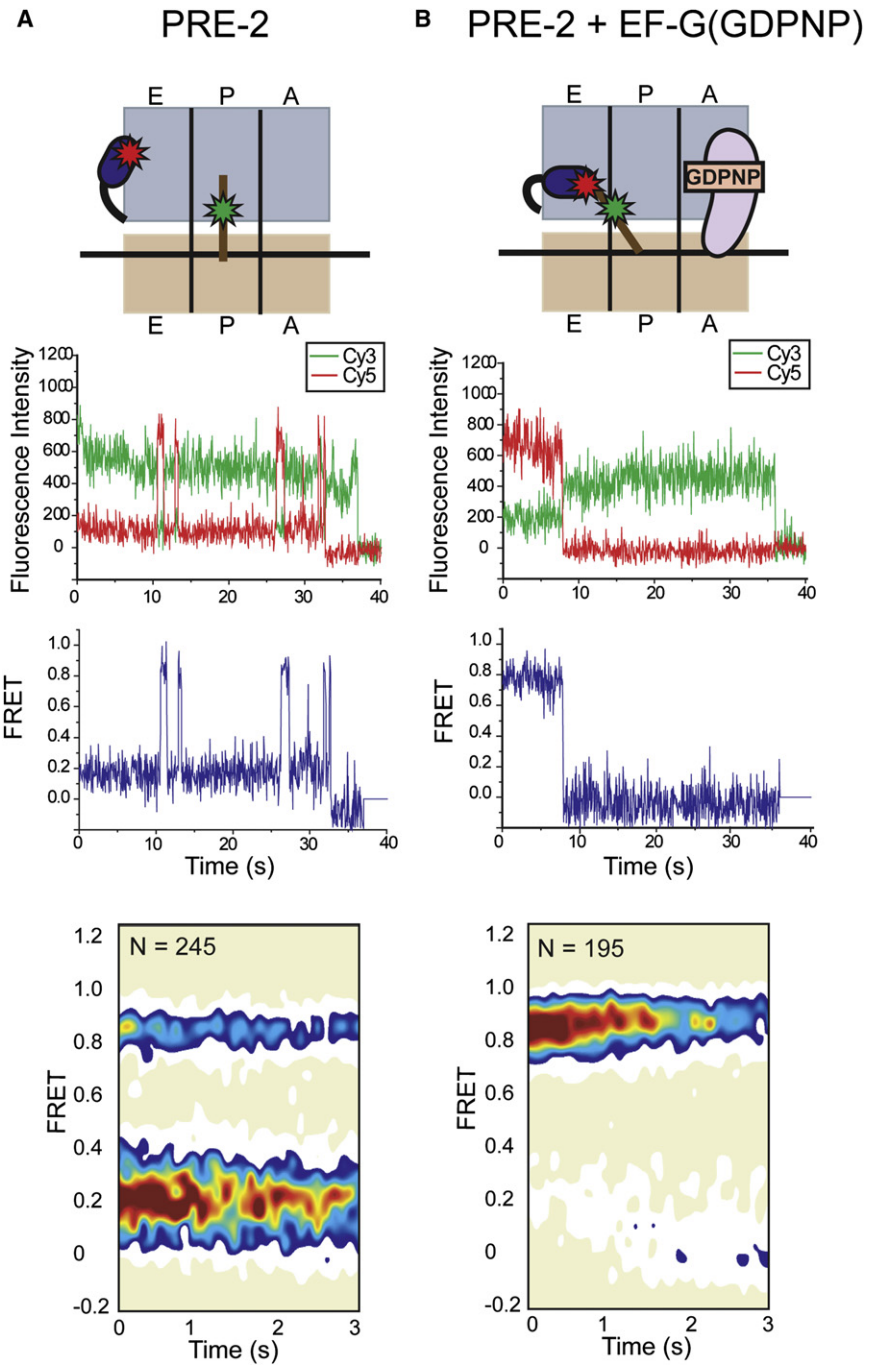

Figure 3. Steady-State smFRET Measurements of PRE-2 in the Absence and Presence of EF-G(GDPNP)

Data are displayed as in Figure 2. (A) PRE-2. (B) PRE-2 stably trapped in the 0.84 FRET state by addition of 1 μM EF-G in the presence of GDPNP.

A Pretranslocation Complex Fluctuates between Two Distinct States

We next reacted POST-1 with EF-Tu(GTP) Lys-tRNA^{Lys} in order to generate a pretranslocation complex (PRE-1), leaving the newly deacylated OH-(Cy3)tRNA^{Phe} in the P site and the newly formed fMet-Phe-Lys-tRNA^{Lys} in the A site. Analysis of the steady-state smFRET traces generated from this pretranslocation complex reveals a fluctuating signal with transitions between two well-defined smFRET states (Figure 2B). The first state is centered at 0.21 FRET, coincident with the average value of the smFRET distribution observed in POST-1 (Figure 2A). The second is a high FRET state centered at 0.84 FRET. This result indicates that a pretranslocation complex exists in a dynamic equilibrium between two conformational states, each encompassing a different distance between the L1 stalk and the OH-(Cy3)tRNA^{Phe}.

Similar smFRET behavior is observed when POST-1 is reacted with the antibiotic puromycin. Puromycin is an analog of the 3′-terminal residue of aminoacyl-tRNA that binds to a vacant A site, participates in the peptidyl transferase reaction, and subsequently dissociates from the ribosome (Traut and Monro, 1964). Puromycin treatment effectively deacylates the P site tRNA and thereby generates a complex with only deacylated OH-(Cy3)tRNA^{Phe} in the P site (PRE-2). As with PRE-1, fluctuations between two smFRET states, centered at 0.21 and 0.84 FRET, are observed in PRE-2 (Figure 3A). The major difference between the two complexes, evident in the smFRET trace shown in Figure 3A, is the extended lifetime of the 0.21 FRET state in PRE-2.

Comparison of contour plots of the time evolution of population FRET reveals that the broad smFRET distribution centered at ~0.2 FRET in POST-1 narrows dramatically in PRE-1 and PRE-2 (Figures 2 and 3). Based on our conclusion that the broad smFRET distribution in POST-1 most likely originates from heterogeneity related to tRNA occupancy of the E site, we suggest that the narrowing of this distribution in PRE-1 and PRE-2 reflects quantitative dissociation of E site tRNA, thereby generating

to changes in distance. It is therefore difficult to resolve individual FRET states for the structural conformations of the L1 stalk relative to the classical P/P tRNA. However, assuming that the available structures accurately reflect the range of motion allowed for the L1 stalk (Harms et al., 2001; Korostelev et al., 2006; Schuwirth et al., 2005; Selmer et al., 2006), our labels on the L1 stalk and the classical P/P tRNA sample a distance range of approximately 70–90 Å, predicting smFRET values for Cy3/Cy5 (with Förster distance of ~50 Å) of 0–0.2 FRET, falling within the broad range of smFRET values experimentally observed here.

a homogeneous population of ribosomal complexes with vacant E sites. This then implies that the E site tRNA dissociates at a point during the elongation cycle that either precedes or is concomitant with formation of the pretranslocation state. Future single-molecule fluorescence experiments, designed to measure the precise timing of E site tRNA release relative to other events in the elongation cycle, should allow testing of this hypothesis.

The L1 Stalk Is Static Relative to the Classical E/E tRNA in a Posttranslocation Complex

We then reacted POST-1 with EF-Tu(GTP)Lys-tRNA^{Lys} and EF-G(GTP) to form a posttranslocation complex (POST-2) that contains deacylated OH-(Cy3)tRNA^{Phe} in the E site, fMet-Phe-Lys-tRNA^{Lys} in the P site, and an empty A site (Figure 1B). This complex yields a single, stable smFRET signal centered at 0.84 FRET (Figure 2C). This smFRET value is consistent with X-ray crystallographic structures of functional 70S complexes in which the L1 stalk is found to make direct contact with the classical E/E tRNA. The observed smFRET signal is very stable, with measurement of the state's actual lifetime limited by the rate of Cy5 photobleaching, indicating that, relative to the E site tRNA, the L1 stalk does not undergo dynamic transitions in a posttranslocation ribosome.

The Low and High FRET States in the Pretranslocation Complex Can Be Assigned to Two Distinct and Structurally Well-Defined Ribosomal Complexes

The 0.21 FRET state observed in PRE-1 and PRE-2 coincides with the average value of ~0.2 FRET observed in POST-1. POST-1 is a structurally well-defined ribosomal complex in which tRNAs are found in the classical configuration, the L1 stalk is positioned away from the intersubunit space, and the ribosomal subunits are in the nonratcheted state (Valle et al., 2003); the observed smFRET signal thus reports on the distance between the L1 stalk and fMet-Phe-(Cy3)tRNA^{Phe} in the classical P/P configuration. Based on the correspondence of their smFRET values, we assigned the 0.21 FRET state in the pretranslocation complexes as representing the nonratcheted state of the ribosome, in which the L1 stalk does not interact with the deacylated classical P/P (Cy3)tRNA^{Phe}. By deduction, we assigned the 0.84 FRET state in the pretranslocation complexes as correlating with the ratcheted state of the ribosome, in which the L1 stalk is positioned toward the intersubunit space and directly contacts the deacylated hybrid P/E (Cy3)tRNA^{Phe}. Our assignment of the ratcheted conformation of the ribosome is supported by recent experiments demonstrating that the ratcheted state of the ribosome can be induced in the absence of EF-G under conditions that favor the hybrid tRNA configuration (Ermolenko et al., 2007).

We confirmed our assignment of the 0.84 FRET state by delivering EF-G, in the presence of the nonhydrolyzable GTP analog, GDPNP, to PRE-2. The complex formed by EF-G(GDPNP) binding to PRE-2 is structurally well-defined, revealing a direct interaction between the L1 stalk and the hybrid P/E tRNA and a ratcheted ribosome (Connell et al., 2007; Valle et al., 2003). Here the observed smFRET signal reports on a direct intermolecular contact between the L1 stalk and OH-(Cy3)tRNA^{Phe} in the hybrid P/E configuration. Our experiments show that, upon binding of EF-G(GDPNP), the fluctuating smFRET signal of PRE-2 is fully resolved to a very stable smFRET signal centered at 0.84 FRET, indistinguishable from the 0.84 FRET state sampled by the fluctuating pretranslocation complex (Figure 3B). The data and assignments presented here demonstrate that, contrary to the interpretation of cryo-EM structures (Valle et al., 2003), the formation of the L1 stalk-P/E tRNA interaction and the relative rotation of the ribosomal subunits occur spontaneously upon peptide bond formation, with no requirement for EF-G binding.

L1 Stalk and Ratcheting Dynamics Are Concerted and Correlate with Fluctuations of the tRNAs between Classical and Hybrid Configurations

At present, the manner in which L1 stalk and ratcheting dynamics are temporally coupled is unknown; concerted, stepwise, or stochastic mechanisms are all possibilities. Furthermore, it is unclear if and how these conformational rearrangements of the ribosome are coupled to tRNA dynamics in the pretranslocation complex. In order to determine how movements of the ribosome and its tRNA substrates are coupled, we analyzed the smFRET transitions in the pretranslocation complex, determined lifetimes of the two smFRET states, and sought to identify any substeps or intermediates in the reaction pathway.

In both PRE-1 and PRE-2, transitions between 0.21 and 0.84 FRET occur within one frame in all smFRET traces, and transition density plots for PRE-1 and PRE-2 (Figures 4A and 4B) clearly demonstrate the existence of just two populations of smFRET transitions (from 0.21 to 0.84 and from 0.84 to 0.21 FRET) with no evidence of any intermediate states, at least at this time resolution (20 frames s^{-1}). In agreement with these results, histograms of dwell times spent in either the 0.21 or the 0.84 FRET state are well described by single-exponential decays, with the exception of the dwell-time histogram of the 0.21 FRET state in PRE-1, which is best described by a double exponential decay. This latter finding is due to the existence of a second population of PRE-1 complexes known to arise from the dissociation of the relatively labile peptidyl-tRNA from the A/P hybrid configuration (Table 1) (Blanchard et al., 2004; Semenkov et al., 2000). Taken together with our FRET state assignments, the lack of detectable intermediates strongly suggests that tRNA, L1 stalk, and ratcheting dynamics are all coupled, each representing a dynamic feature of the same global conformational change of the pretranslocation complex.

The lifetime of the 0.21 FRET state in PRE-1 is 0.22 ± 0.02 s (Figure 4A, Table 1) and correlates almost exactly with the lifetime of the classical tRNA configuration measured using a tRNA-tRNA smFRET signal in a similar pretranslocation complex (τ = 0.20 ± 0.02 s) (Blanchard et al., 2004). Likewise, the lifetime of 0.78 ± 0.03 s for the 0.84 FRET state (Figure 4A, Table 1) is consistent with the previously reported lifetime of the hybrid tRNA configuration (τ = 0.39 ± 0.01 s) (Blanchard et al., 2004). The 2-fold longer lifetime of the hybrid P/E configuration observed in the present study is most likely related to differences in the tRNAs used in the two studies. The experiments described here use tRNA^{Phe} and tRNA^{Lys} in the P and A sites, respectively, versus tRNA^{fMet} and tRNA^{Phe} in the corresponding sites in the

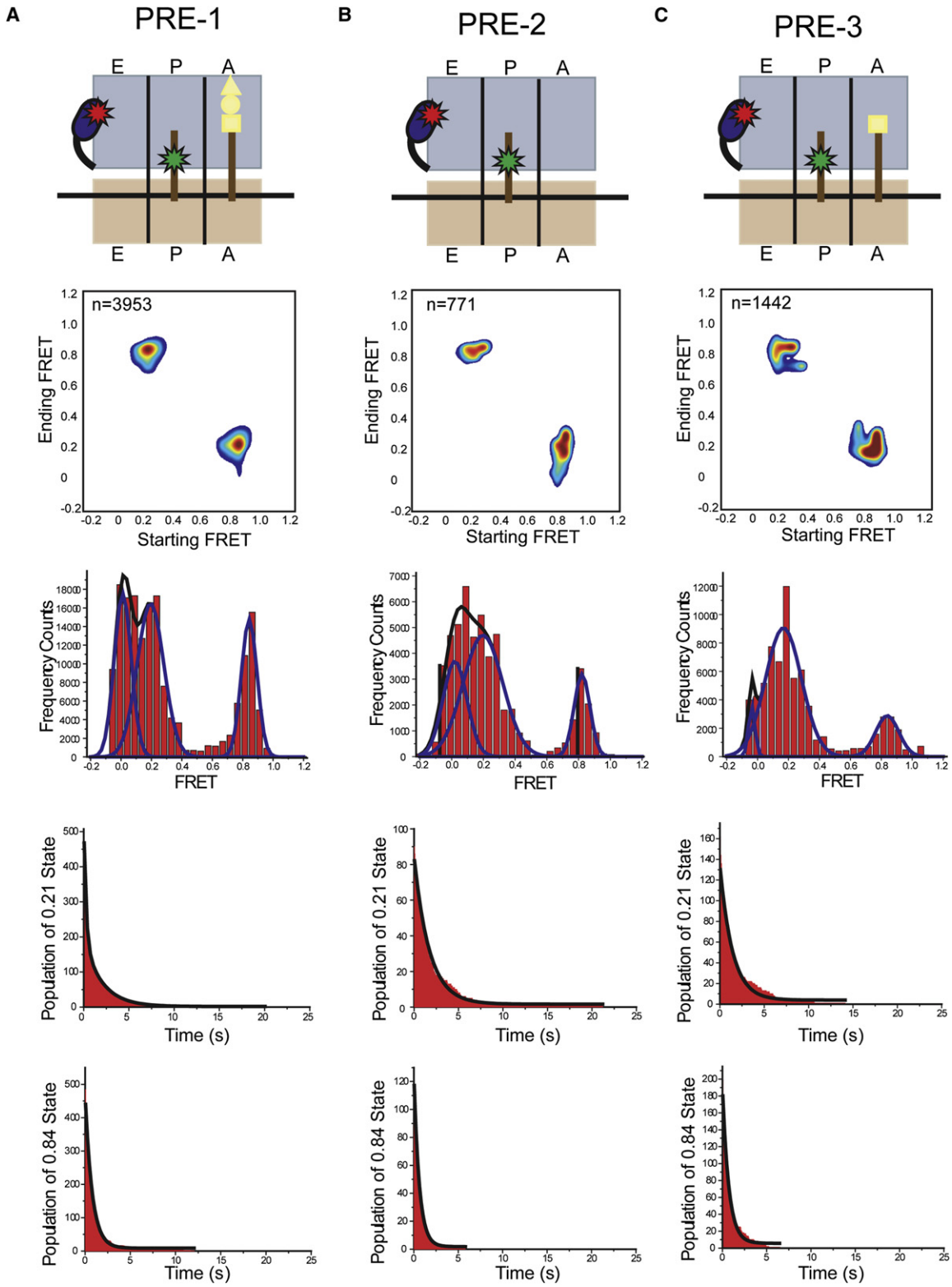

Figure 4. Lifetime Analyses of PRE-1, PRE-2, and PRE-3

Cartoons for each complex are depicted as described in Figures 2 and 3 (first row). Transition density plots for each complex are generated by plotting the "Starting FRET" versus "Ending FRET" for each transition as contour plots of two-dimensional population histograms. Contours are plotted from tan (lowest population) to red (highest population). The number of transitions that were used to construct each contour plot is indicated by "n" (second row). One-dimensional

Table 1. Contributions of the A Site tRNA and Its Acylation State to the Lifetimes of the 0.21 FRET/GS1 and 0.84 FRET/GS2 States

Complex	A Site Substrate	$\tau_{0.21/GS1}$ (s)	$\tau_{0.84/GS2}$ (s)
PRE-1	fMet-Phe-Lys-tRNA^{Lys}	0.22 ± 0.02[a,b]	0.78 ± 0.03[a]
PRE-2	Empty A site	1.60 ± 0.1[a]	0.59 ± 0.02[a]
PRE-3	Lys-tRNA^{Lys}	1.30 ± 0.1[a]	0.75 ± 0.04[a]

[a] Lifetimes reported here are the average and standard deviation of three independent fits to histograms of time spent in GS1 and GS2 where the thresholds defining GS1 and GS2 were varied as described in the Lifetime Analysis section of the Experimental Procedures.

[b] All decay curves were well-described by single exponential fits, with the exception of the GS1 state of PRE-1, which is better described by a double exponential decay. The lifetime reported here for the GS1 state of PRE-1 is the fast population (~60%). The slow population (~40%) lifetime is 1.97 ± 0.03 s. As in smFRET studies of tRNA dynamics (Blanchard et al., 2004), this slow population is assigned to complexes in which the peptidyl-tRNA has dissociated from the A/P hybrid state, which is known to be unstable in the pretranslocation complex (Semenkov et al., 2000). The population of complexes in which the peptidyl-tRNA has dissociated from the A/P hybrid state is identical to PRE-2. Setting the lifetime of the slow population to 1.6 s, to reflect the $\tau_{0.21/GS1}$ of PRE-2, and repeating the double exponential fitting generates a lifetime of 0.18 ± 0.02 s for the fast population of PRE-1 (within error of the $\tau_{0.21/GS1}$ of PRE-1 reported in Table 1) without any decrease in the goodness of fit, R^2.

previous study (Blanchard et al., 2004). tRNA^{fMet} has a reported lower propensity to form the hybrid P/E configuration than tRNA^{Phe} (Dorner et al., 2006; Ermolenko et al., 2007; Studer et al., 2003), and comparison of the lifetimes reported above suggests that the origin of this effect is a destabilization of the hybrid P/E configuration of tRNA^{fMet}. Direct correlation of the lifetimes of the 0.21 and 0.84 FRET states with the lifetimes of the classical and hybrid tRNA configurations lends further evidence to our claim that the classical-to-hybrid tRNA transition, establishment of the L1 stalk-tRNA interaction, and relative rotation of the ribosomal subunits into the ratcheted state are all coupled.

In summary, we propose that the entire pretranslocation ribosomal complex fluctuates, through a concerted mechanism, between just two global conformational states: global state 1 (GS1), characterized by the classical configuration of the tRNAs, no interaction between the L1 stalk and the deacylated P/P tRNA, a nonratcheted state of the ribosomal subunits, and a low (0.21) FRET signal; and global state 2 (GS2), characterized by the hybrid configuration of the tRNAs, a direct interaction between the L1 stalk and the deacylated P/E tRNA, a ratcheted state of the ribosomal subunits, and a high (0.84) FRET signal. GS1 and GS2 correspond directly to the two ribosomal conformations that have been visualized by cryo-EM in the absence and presence of EF-G, respectively (Valle et al., 2003). Here we demonstrate that the pretranslocation complex exists in a dynamic equilibrium between these two global conformational states, with the L1 stalk, ribosomal subunits, and tRNAs undergoing concerted movements that are independent of EF-G binding and are solely driven by thermal fluctuations.

The Presence of an A Site tRNA, and Its Acylation State, Influences the Energetics of the Pretranslocation Conformational Equilibrium

The L1 stalk-tRNA smFRET signal presented here can be generated either in the absence or presence of an A site-bound tRNA. This allows determination of the influence of an A site tRNA substrate, and its acylation state, on the energetics of the pretranslocation conformational equilibrium. As reported above, the GS1 and GS2 lifetimes of PRE-1 are 0.22 ± 0.02 s and 0.78 ± 0.03 s, respectively (Figure 4A, Table 1). The same measurements on PRE-2 yield a lifetime of 1.6 ± 0.1 s for GS1 and a lifetime of 0.59 ± 0.02 s for GS2 (Figure 4B, Table 1). The presence of a peptidyl-tRNA in the A site therefore shifts the equilibrium toward GS2; this is driven primarily through a 7.3-fold destabilization of GS1 and may be slightly assisted by a small 1.3-fold increase in the lifetime of GS2.

In order to determine the energetic contribution from the acylation state of the A site tRNA, we generated a new pretranslocation complex (PRE-3) by first treating POST-1 with puromycin and then delivering EF-Tu(GTP)Lys-tRNA^{Lys}. Complex PRE-3 therefore carries OH-(Cy3)tRNA^{Phe} at the P site and Lys-tRNA^{Lys} at the A site. In this complex, the GS1 and GS2 lifetimes are 1.3 ± 0.1 s and 0.75 ± 0.04 s, respectively (Figure 4C, Table 1). Consistent with results obtained from monitoring the classical-hybrid tRNA equilibrium using a tRNA-tRNA smFRET signal (Blanchard et al., 2004), our results demonstrate that the pretranslocation conformational equilibrium is sensitive to the acylation state of the A site tRNA (comparing PRE-1 and PRE-3), with peptidyl-tRNA shifting the equilibrium toward GS2 primarily by destabilizing GS1 by approximately 6-fold relative to aminoacyl-tRNA.

In summary, comparison of GS1 and GS2 lifetimes in PRE-1, PRE-2, and PRE-3 demonstrates that GS2 may be slightly stabilized by occupancy of the A site with a tRNA substrate but is essentially insensitive to the tRNA's acylation state. The stability of GS1, on the other hand, is significantly affected by the acylation state of the A site tRNA. The presence of an aminoacyl-tRNA at the A site results in a modest destabilization of GS1; this destabilization increases by approximately 6-fold when the aminoacyl-tRNA is substituted with a peptidyl-tRNA. These energetic effects combine in order to regulate the overall GS1-GS2 equilibrium: in the absence of an A site tRNA, the GS1 conformation is favored, whereas a peptidyl-tRNA at the A site shifts the equilibrium to favor the GS2 conformation.

histograms of idealized smFRET generated from hidden Markov modeling using the HaMMy software suite (McKinney et al., 2006) (third row). Thresholds for each smFRET state were determined by fitting these histograms to three Gaussian distributions with user-specified initial guess values of 0, 0.2, and 0.8 FRET for the Gaussian centers. Population histograms of dwell times in the 0.21 FRET state are well-described by a single exponential decay ($A^*\exp[-t/t_0] + y_0$), with the exception of PRE-1, which is best described by a double exponential decay ($A_1^*\exp[-t/t_1] + A_2 * \exp[-t/t_2] + y_0$) (fourth row). Population histograms of dwell times in the 0.84 FRET state are well described by a single exponential decay (fifth row). (A) PRE-1. (B) PRE-2. (C) PRE-3. Lifetimes are shown in Table 1. The R^2 of all fits was greater than 0.97.

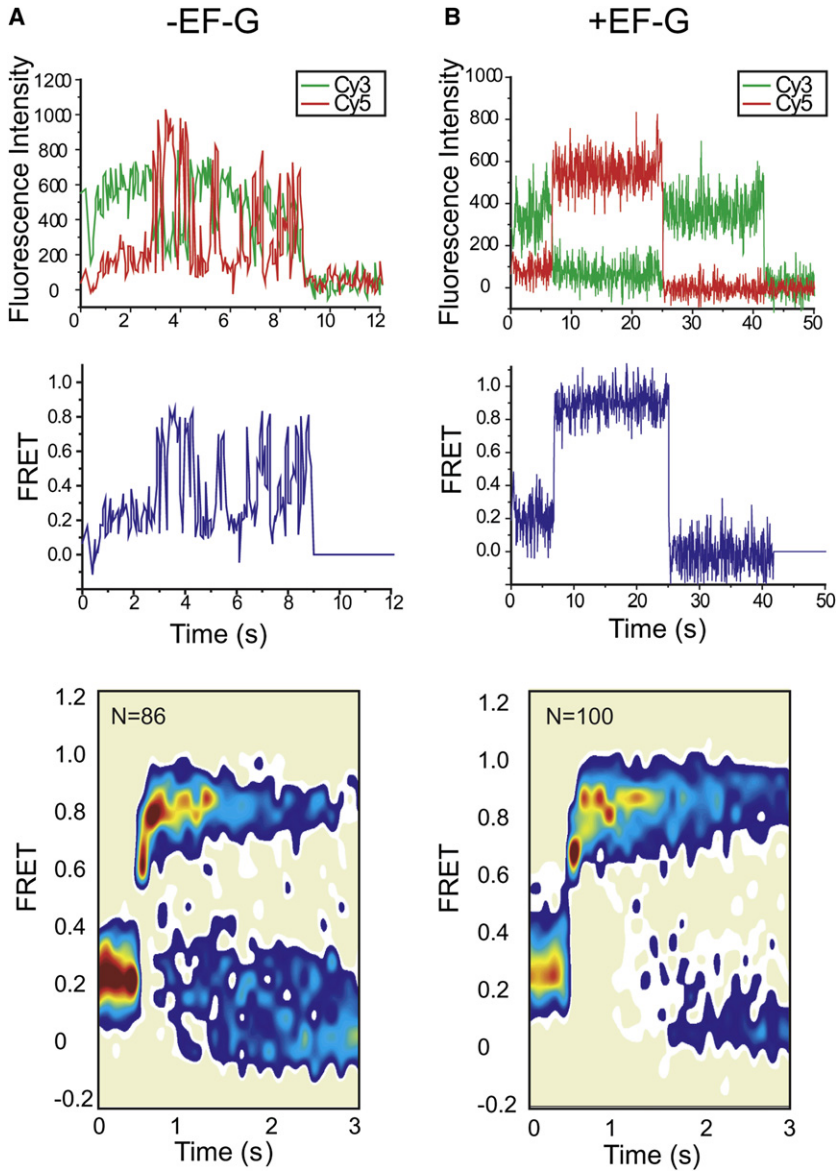

Figure 5. Real-Time smFRET Measurements during Translation Elongation

Real-time stopped-flow delivery of 100 nM EF-Tu(GTP) Lys-tRNA^{Lys} in the presence and absence of 1 μM EF-G(GTP) to surface-immobilized POST-1. Cy3 and Cy5 emission intensities are shown in green and red, respectively (upper row). The corresponding smFRET traces, $I_{Cy5}/(I_{Cy3} + I_{Cy5})$, are shown in blue (middle row). Contour plots of the postsynchronized time evolution of population FRET are generated by superimposing the individual smFRET time traces after synchronizing all traces to the data point 0.5 s (i.e., ten frames) prior to the first FRET value > 0.62. Contours are plotted from tan (lowest population) to red (highest population). Molecules in the FRET = 0 state arise from photobleaching of Cy5. The number of traces that were used to construct each contour plot is indicated by "N." (A) −EF-G. (B) +EF-G.

The Intermolecular Contacts between the L1 Stalk and the Elbow of the Hybrid P/E tRNA Are Identical to Those between the L1 Stalk and the Classical E/E tRNA

Although the ribosomal complexes visualized by cryo-EM in the presence of EF-G(GDPNP) have vacant A sites and are therefore not authentic substrates for the translocation reaction (Connell et al., 2007; Frank and Agrawal, 2000; Valle et al., 2003), these structures have suggested that the molecular interactions between the L1 stalk and the hybrid P/E tRNA are similar, if not identical, to those seen at atomic resolution between the L1 stalk and the classical E/E tRNA (Connell et al., 2007; Korostelev et al., 2006; Li and Frank, 2007; Selmer et al., 2006; Valle et al., 2003). Our smFRET data on an identical complex (PRE-2 in the presence of EF-G[GDPNP]) are entirely consistent with this finding, yielding a 0.84 FRET state that is identical to the 0.84 FRET state observed in POST-2. In addition to confirming the cryo-EM interpretation, we observe that the 0.84 FRET state is identical in PRE-1, PRE-2 (in both the presence and absence of EF-G[GDPNP]), PRE-3, and POST-2, extending this interpretation to complexes that are genuine substrates in the translocation reaction, and demonstrating that the L1 stalk-P/E tRNA interaction is not affected by binding of EF-G.

The L1 Stalk Maintains Its Contacts with the Hybrid P/E tRNA throughout Translocation, Escorting the tRNA into the Classical E/E Configuration

In order to monitor the real-time interaction of the L1 stalk with the P site tRNA during an entire elongation cycle, we stopped-flow delivered EF-Tu(GTP)Lys-tRNA^{Lys} in the presence and absence of EF-G(GTP) to POST-1 and monitored the real-time evolution of smFRET resulting from peptide bond formation and translocation. In both the presence and absence of EF-G(GTP), the smFRET traces reveal a sharp transition from 0.21 to 0.84 FRET. All traces were postsynchronized relative to this transition and used to generate contour plots of the time evolution of population FRET (Figure 5) (Blanchard et al., 2004). This transition occurs within one frame in all traces, independent of the presence or absence of EF-G, consistent with the absence of any intermediate states. In the absence of EF-G, the signal arrives at 0.84 FRET and subsequently begins to fluctuate between 0.21 and 0.84 FRET (Figure 5A), as is characteristic of the pretranslocation complex (PRE-1, Figure 2B). In contrast, in the presence of EF-G(GTP), the signal reaches and remains stably centered at 0.84 FRET (Figure 5B). This is strong evidence supporting a model in which the L1 stalk remains associated with the hybrid P/E tRNA during translocation and its concomitant reconfiguration into the classical E/E site.

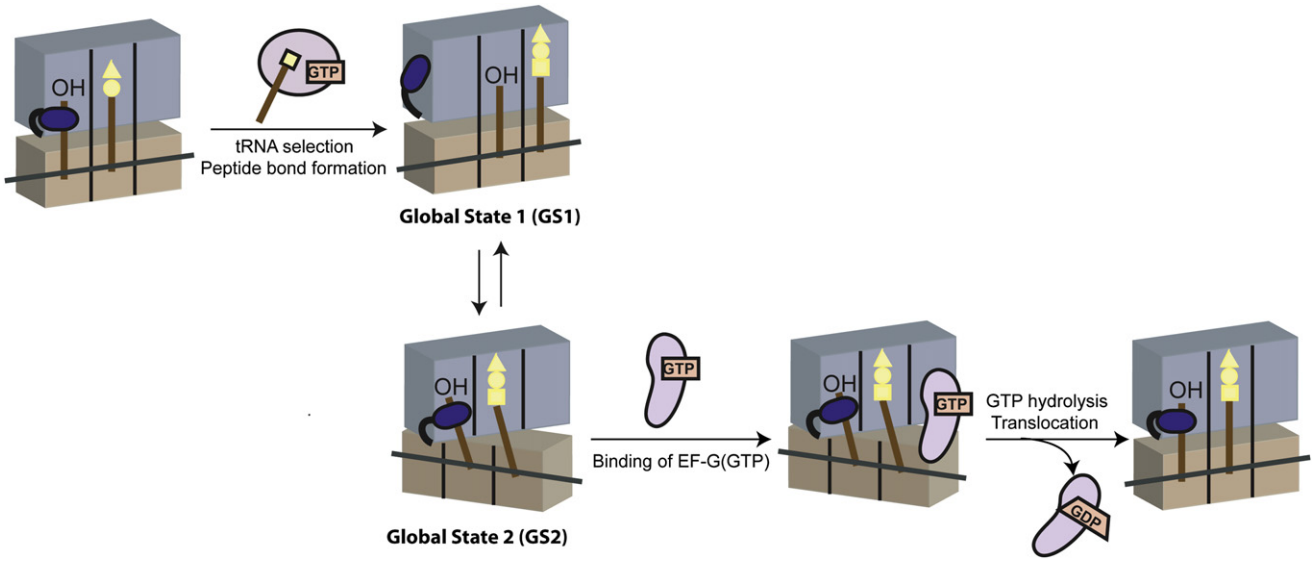

Figure 6. Model for L1 Stalk-tRNA Dynamic Coupling during Translation Elongation

The L1 stalk (dark blue) interaction with the newly deacylated P site tRNA (brown) is established spontaneously upon peptide bond formation. This event is the consequence of a concerted conformational change of the tRNAs (brown) and the ribosome (30S in tan and 50S in lavender) that involves the classical-to-hybrid transition of the tRNAs, movement of the L1 stalk into the intersubunit space, and relative rotation of the ribosomal subunits into the ratcheted state. In the absence of EF-G (light purple), formation of the L1 stalk-P/E tRNA intermolecular contact is inherently reversible. The contact alternately breaks and reforms concomitantly with coupled fluctuations of the entire pretranslocation complex between two distinct global conformational states, GS1 and GS2. EF-G does not catalyze the GS1-to-GS2 transition; instead, binding of EF-G to GS2 provides directionality to the pretranslocation equilibrium by stabilizing this state and blocking the GS2-to-GS1 transition. The L1 stalk-P/E tRNA interaction, which is maintained throughout EF-G catalyzed GTP hydrolysis and subsequent translocation of the tRNA anticodon-mRNA codon complex on the 30S subunit, collaborates with EF-G in directing the inherently stochastic movement of the tRNAs during translocation.

The Mechanistic Role of L1 Stalk Conformational Dynamics during Translocation

The interaction between the L1 stalk of the ribosome and the P site tRNA is established spontaneously and rapidly upon peptide bond formation. This event is the consequence of a concerted conformational change of the tRNAs and the ribosome that involves the classical-to-hybrid transition of the tRNAs, movement of the L1 stalk into the intersubunit space, and relative rotation of the ribosomal subunits into the ratcheted state. In the absence of EF-G, formation of the L1 stalk-P/E tRNA intermolecular contact is inherently reversible; the contact alternately breaks and reforms in concert with fluctuations of the pretranslocation complex between two distinct global conformational states, GS1 and GS2 (Figure 6).

The rate of the GS1-to-GS2 transition is $\sim$4.5 s^{-1} at 25°C (Figure 4 and Table 1), slightly faster than the 1 s^{-1} rate of translocation measured under similar conditions at 25°C (Studer et al., 2003), suggesting that EF-G may not necessarily catalyze the GS1-to-GS2 transition. Indeed, a preliminary dwell-time analysis of our real-time stopped-flow smFRET experiments (Figure 5) is consistent with an insignificant contribution from EF-G(GTP) to the dwell time between stopped-flow delivery of EF-Tu(GTP) Lys-$tRNA^{Lys}$ and initial detection of the 0.21-to-0.84 FRET transition. Based on these results, we speculate that EF-G does not catalyze the GS1-to-GS2 transition. Instead, we favor a model in which EF-G imparts directionality to the translocation reaction by specifically recognizing and binding GS2, thereby stabilizing the pretranslocation complex in this state and effectively blocking the GS2-to-GS1 transition (Figure 6).

The role we ascribe to EF-G in directing the GS1-GS2 equilibrium bears striking similarities to recent proposals for a role of EF-G in directing the intrinsically stochastic movement of the tRNA anticodon-mRNA codon complex within the 30S subunit (Konevega et al., 2007; Savelsbergh et al., 2003; Shoji et al., 2006; Wintermeyer et al., 2004). These proposals stipulate that EF-G acts as a Brownian motor, coupling hydrolysis of GTP to a conformational rearrangement of the ribosome-EF-G(GDP•P_i) complex that "unlocks" the pretranslocation ribosome. Subsequent to the unlocking step, EF-G(GDP•P_i) is hypothesized to direct the inherently Brownian motion of the tRNA anticodon-mRNA codon complex in the forward direction primarily by blocking movement in the reverse direction (Savelsbergh et al., 2003; Wintermeyer et al., 2004). We extend these ideas further and propose that the ribosomal L1 stalk collaborates with EF-G in directing the movement of the tRNAs during translocation. Based on our observation that the interaction between the L1 stalk and the hybrid P/E tRNA is maintained upon GTP hydrolysis by EF-G and translocation of the anticodon ends of the tRNAs on the 30S subunit, we propose that the L1 stalk aids in biasing the stochastic motion of the hybrid P/E tRNA toward the classical E/E site. Support for the vital role that the L1 stalk-tRNA interaction plays in the mechanism of translocation is provided by the observation that mutations in the vicinity of the G19-C56 base pair of the tRNA elbow, which directly contacts the L1 stalk

(Korostelev et al., 2006), lead to an 80-fold reduction in the rate of translocation (Pan et al., 2006). Future smFRET experiments incorporating ribosomal mutations designed to disrupt the L1 stalk-tRNA interaction should allow further insight into the role of the L1 stalk in directing tRNA movement during translocation.

EXPERIMENTAL PROCEDURES

Buffer Conditions

All single-molecule experiments were performed in Tris-polymix buffer (50 mM Tris-OAc, 100 mM KCl, 5 mM NH_4OAc, 0.5 mM $Ca[OAc]_2$, 6 mM 2-mercaptoethanol, 5 mM putrescine, and 1 mM spermidine) at 15 mM $Mg(OAc)_2$ and $pH_{25°C}$ 7.5, supplemented with an oxygen-scavenging system (25 units/mL glucose oxidase, 250 units/μl catalase, and 1% β-D-glucose). In addition, 1,3,5,7-cyclooctatetraene (Aldrich) and p-nitrobenzyl alcohol (Fluka) were added to all buffers in order to quench a long-lived nonfluorescent triplet state sampled by the Cy5 fluorescent dye (Blanchard et al., 2004; Gonzalez et al., 2007). Biochemical experiments were performed under identical buffer conditions with the exception that the oxygen-scavenging and triplet state quencher systems were omitted. Previous biochemical experiments have demonstrated that the oxygen-scavenging and triplet state quencher systems have no effect on our in vitro translation system (Blanchard et al., 2004; Gonzalez et al., 2007).

Posttranslocation Complex Formation and Purification

The posttranslocation elongation complex (complex POST-1) was prepared in three steps. In the first step, L1(Cy5) ribosomes were incubated with initiation factors, fMet-$tRNA^{fMet}$, and a 5′-biotinylated mRNA to enzymatically form an initiation complex containing fMet-$tRNA^{fMet}$ in the P site. This initiation complex was then put through one elongation cycle by adding EF-Tu(GTP) Phe-(Cy3)$tRNA^{Phe}$ along with EF-G(GTP). The resulting elongated posttranslocation 70S complex was separated from free mRNA, translation factors, and aminoacyl-tRNAs by sucrose density gradient ultracentrifugation as previously described (Blanchard et al., 2004).

Surface Immobilization of Fluorescent Ribosome Complexes

Quartz microscope slides were cleaned and derivatized with a mixture of polyethyleneglycol (PEG) and PEG-biotin in order to passivate the quartz surface as previously described (Blanchard et al., 2004). Just prior to smFRET experiments, the slides were treated with streptavidin, and purified elongation complexes were immobilized via the biotinylated mRNA (Blanchard et al., 2004).

Total Internal Reflection Fluorescence Microscopy

We have designed and constructed a wide-field, prism-based, total internal reflection fluorescence microscope utilizing a 150 mW diode-pumped 532 nm laser (CrystaLaser), set at 18 mW, as an excitation source and a back-thinned charged coupled device (Cascade II, Princeton Instruments) as a detector. This microscope allows direct visualization of approximately 100–200 ribosomal complexes in an observation area of 60 × 60 μm. The penetration depth of the evanescent field generated by total internal reflection at the interface between the quartz microscope slide and aqueous buffer containing our sample is approximately 150–200 nm. Dissociation of fluorescent tRNAs from the E site of surface-immobilized ribosomes was monitored by a loss of fluorescence intensity due to rapid diffusion of the dissociated fluorescent tRNA from the evanescent excitation field. For smFRET experiments, a Quad-View (Optical Insights, Inc.) multichannel imaging system allows simultaneous acquisition of both the Cy3 donor and Cy5 acceptor channels in a single exposure. The time resolution of smFRET measurements is 50 ms per frame. Single ribosomes are characterized by single-step photobleaching of the fluorophores.

Lifetime Analysis

Each smFRET trajectory was fit to a hidden Markov model by using the HaMMy software suite (McKinney et al., 2006) with an initial guess of five states. The resulting idealized trajectories were filtered by two criteria: transitions occurring with a change in smFRET of less than 0.1 were discarded, as were transitions lasting a single frame. Dwell times in each state before a transition were extracted from the idealized smFRET trajectories. Due to the arbitrary onset of data collection and the stochastic nature of the photobleaching event, dwell times from the first and last transitions were not included in the analysis. For each complex, one-dimensional histograms of smFRET values were plotted by using all of the data points from the entire set of idealized smFRET traces. Each histogram was fit to three Gaussian distributions by using Origin 7.0 and user-specified initial guess values of 0, 0.2, and 0.8 for the Gaussian centers. Initial thresholds for each state were set by using the full width at half height of the Gaussian distributions. These thresholds were 0.08–0.30 FRET for GS1 and 0.78–0.90 FRET for GS2. One-dimensional histograms of time spent in GS1 and GS2 were plotted and lifetimes were determined by fitting each histogram to a single or double exponential decay. Thresholds were then increased and decreased by a full standard deviation of the original Gaussian fits to test the sensitivity of the calculated lifetimes to the choice of thresholds. The increased thresholds were 0.11–0.33 FRET for GS1 and 0.79–0.91 FRET for GS2. The decreased thresholds were 0.05–0.26 FRET for GS1 and 0.76–0.88 FRET for GS2. The sensitivity to threshold values was found to be insignificant. The final reported lifetimes in Table 1 are the average values and standard deviations calculated from these three sets of thresholds.

SUPPLEMENTAL DATA

Supplemental Data include Supplemental Experimental Procedures, four figures, and Supplemental References and can be found with this article online at http://www.molecule.org/cgi/content/full/30/3/348/DC1/.

ACKNOWLEDGMENTS

This work was supported in part by start-up funds to R.L.G. from Columbia University and grants to R.L.G. from the Burroughs Wellcome Fund (CABS 1004856) and the U.S. National Science Foundation (MCB 0644262). We are indebted to Mr. Benjamin Cahan and Ms. Subhasree Das for managing the laboratory and to Prof. Barry L. Wanner for the kind gift of the plasmids and strains required for the L1 gene deletion. We thank Prof. Joachim Frank and Prof. Eric C. Greene, as well as the members of the Gonzalez laboratory, for carefully reading the manuscript and providing valuable comments.

Received: October 31, 2007
Revised: March 14, 2008
Accepted: March 28, 2008
Published: May 8, 2008

REFERENCES

Blanchard, S.C., Kim, H.D., Gonzalez, R.L., Jr., Puglisi, J.D., and Chu, S. (2004). tRNA dynamics on the ribosome during translation. Proc. Natl. Acad. Sci. USA *101*, 12893–12898.

Connell, S.R., Takemoto, C., Wilson, D.N., Wang, H., Murayama, K., Terada, T., Shirouzu, M., Rost, M., Schuler, M., Giesebrecht, J., et al. (2007). Structural basis for interaction of the ribosome with the switch regions of GTP-bound elongation factors. Mol. Cell *25*, 751–764.

Dorner, S., Brunelle, J.L., Sharma, D., and Green, R. (2006). The hybrid state of tRNA binding is an authentic translation elongation intermediate. Nat. Struct. Mol. Biol. *13*, 234–241.

Ermolenko, D.N., Majumdar, Z.K., Hickerson, R.P., Spiegel, P.C., Clegg, R.M., and Noller, H.F. (2007). Observation of intersubunit movement of the ribosome in solution using FRET. J. Mol. Biol. *370*, 530–540.

Frank, J., and Agrawal, R.K. (2000). A ratchet-like inter-subunit reorganization of the ribosome during translocation. Nature *406*, 318–322.

Gonzalez, R.L., Jr., Chu, S., and Puglisi, J.D. (2007). Thiostrepton inhibition of tRNA delivery to the ribosome. RNA *13*, 2091–2097.

Harms, J., Schluenzen, F., Zarivach, R., Bashan, A., Gat, S., Agmon, I., Bartels, H., Franceschi, F., and Yonath, A. (2001). High-resolution structure of the large ribosomal subunit from a mesophilic eubacterium. Cell *107*, 679–688.

Hartz, D., McPheeters, D.S., Traut, R., and Gold, L. (1988). Extension inhibition analysis of translation initiation complexes. Methods Enzymol. *164*, 419–425.

Kim, H.D., Puglisi, J., and Chu, S. (2007). Fluctuations of transfer RNAs between classical and hybrid states. Biophys. J. *93*, 3575–3582.

Konevega, A.L., Fischer, N., Semenkov, Y.P., Stark, H., Wintermeyer, W., and Rodnina, M.V. (2007). Spontaneous reverse movement of mRNA-bound tRNA through the ribosome. Nat. Struct. Mol. Biol. *14*, 318–324.

Korostelev, A., Trakhanov, S., Laurberg, M., and Noller, H.F. (2006). Crystal structure of a 70S ribosome-tRNA complex reveals functional interactions and rearrangements. Cell *126*, 1065–1077.

Li, W., and Frank, J. (2007). Transfer RNA in the hybrid P/E state: correlating molecular dynamics simulations with cryo-EM data. Proc. Natl. Acad. Sci. USA *104*, 16540–16545.

McKinney, S.A., Joo, C., and Ha, T. (2006). Analysis of single-molecule FRET trajectories using hidden Markov modeling. Biophys. J. *91*, 1941–1951.

Moazed, D., and Noller, H.F. (1989). Intermediate states in the movement of transfer RNA in the ribosome. Nature *342*, 142–148.

Munro, J.B., Altman, R.B., O'Connor, N., and Blanchard, S.C. (2007). Identification of two distinct hybrid state intermediates on the ribosome. Mol. Cell *25*, 505–517.

Odom, O.W., Picking, W.D., and Hardesty, B. (1990). Movement of tRNA but not the nascent peptide during peptide bond formation on ribosomes. Biochemistry *29*, 10734–10744.

Pan, D., Kirillov, S., Zhang, C.M., Hou, Y.M., and Cooperman, B.S. (2006). Rapid ribosomal translocation depends on the conserved 18-55 base pair in P-site transfer RNA. Nat. Struct. Mol. Biol. *13*, 354–359.

Savelsbergh, A., Katunin, V.I., Mohr, D., Peske, F., Rodnina, M.V., and Wintermeyer, W. (2003). An elongation factor G-induced ribosome rearrangement precedes tRNA-mRNA translocation. Mol. Cell *11*, 1517–1523.

Schuwirth, B.S., Borovinskaya, M.A., Hau, C.W., Zhang, W., Vila-Sanjurjo, A., Holton, J.M., and Cate, J.H.D. (2005). Structures of the bacterial ribosome at 3.5 Å resolution. Science *310*, 827–834.

Selmer, M., Dunham, C.M., Murphy, F.V., IV, Weixlbaumer, A., Petry, S., Kelley, A.C., Weir, J.R., and Ramakrishnan, V. (2006). Structure of the 70S ribosome complexed with mRNA and tRNA. Science *313*, 1935–1942.

Semenkov, Y.P., Rodnina, M.V., and Wintermeyer, W. (1996). The "allosteric three-site model" of elongation cannot be confirmed in a well-defined ribosome system from *Escherichia coli*. Proc. Natl. Acad. Sci. USA *93*, 12183–12188.

Semenkov, Y.P., Rodnina, M.V., and Wintermeyer, W. (2000). Energetic contribution of tRNA hybrid state formation to translocation catalysis on the ribosome. Nat. Struct. Biol. *7*, 1027–1031.

Shoji, S., Walker, S.E., and Fredrick, K. (2006). Reverse translocation of tRNA in the ribosome. Mol. Cell *24*, 931–942.

Spirin, A.S. (1985). Ribosomal translocation: facts and models. Prog. Nucleic Acid Res. Mol. Biol. *32*, 75–114.

Studer, S.M., Feinberg, J.S., and Joseph, S. (2003). Rapid kinetic analysis of EF-G-dependent mRNA translocation in the ribosome. J. Mol. Biol. *327*, 369–381.

Traut, R.R., and Monro, R.E. (1964). The puromycin reaction and its relation to protein synthesis. J. Mol. Biol. *10*, 63–72.

Valle, M., Zavialov, A.V., Sengupta, J., Rawat, U., Ehrenberg, M., and Frank, J. (2003). Locking and unlocking of ribosomal motions. Cell *114*, 123–134.

Wintermeyer, W., Peske, F., Beringer, M., Gromadski, K.B., Savelsbergh, A., and Rodnina, M.V. (2004). Mechanisms of elongation on the ribosome: dynamics of a macromolecular machine. Biochem. Soc. Trans. *32*, 733–737.

Yusupov, M.M., Yusupova, G.Z., Baucom, A., Lieberman, K., Earnest, T.N., Cate, J.H., and Noller, H.F. (2001). Crystal structure of the ribosome at 5.5 Å resolution. Science *292*, 883–896.